JP Journal of Heat and Mass Transfer

https://pphmjopenaccess.com
https://doi.org/10.17654/0973576325004
Volume 38, Number 1, 2025, Pages 77-94 **P-ISSN: 0973-5763**

STABILITY ANALYSIS ON REINER-PHILLIPPOFF HYBRID NANOFLUID FLOW OVER A WEDGE

Iskandar Waini[1,*], Khairum Bin Hamzah[1], Najiyah Safwa Khashi'ie[2], Nurul Amira Zainal[2], Abdul Rahman Mohd Kasim[3], Anuar Ishak[4] and Ioan Pop[5]

[1]Fakulti Teknologi dan Kejuruteraan Industri dan Pembuatan
Universiti Teknikal Malaysia Melaka
Hang Tuah Jaya, 76100 Durian Tunggal
Melaka, Malaysia

[2]Fakulti Teknologi dan Kejuruteraan Mekanikal
Universiti Teknikal Malaysia Melaka
Hang Tuah Jaya, 76100 Durian Tunggal
Melaka, Malaysia

[3]Centre for Mathematical Sciences
Universiti Malaysia Pahang Al-Sultan Abdullah
Lebuh Persiaran Tun Khalil Yaakob
Gambang, Kuantan, 26300, Pahang, Malaysia

Received: October 1, 2024; Accepted: November 15, 2024
Keywords and phrases: hybrid nanofluid, Reiner-Phillippoff, stability analysis, wedge.
*Corresponding author
Communicated by K. K. Azad

How to cite this article: Iskandar Waini, Khairum Bin Hamzah, Najiyah Safwa Khashi'ie, Nurul Amira Zainal, Abdul Rahman Mohd Kasim, Anuar Ishak and Ioan Pop, Stability analysis on Reiner-Phillippoff hybrid nanofluid flow over a wedge, JP Journal of Heat and Mass Transfer 38(1) (2025), 77-94. https://doi.org/10.17654/0973576325004

Published Online: January 4, 2025

[4]Department of Mathematical Sciences
Faculty of Science and Technology
Universiti Kebangsaan Malaysia
43600 UKM Bangi, Selangor, Malaysia

[5]Department of Mathematics
Babeş-Bolyai University
Cluj-Napoca, 400084, Romania

Abstract

This paper reports on the fluid flow characteristics as well as the heat transfer attribute of a Reiner-Philippoff (RP) fluid past a permeable shrinking wedge with a particular focus on the incorporation of the AA7075-AA7072/methanol hybrid nanofluid. Through the application of suitable transformations, the original model in partial differential equations (PDEs) is converted into ordinary differential equations (ODEs) of a specific form. The ODEs are then solved using the bvp4c solver in MATLAB software. The findings showed that when the magnitude of the magnetic parameter is increased, skin friction and heat transfer rate both are increased. Moreover, the inclusion of hybrid nanoparticles has a positive impact on the system, leading to a 6.16% increment in magnitude of skin friction while boosted about 24% improvement in thermal performance. The confirmation of dual solutions leads to a study of stability analysis to examine the reliability of the first solution. It is important to note that the current findings are novel and original for the study of RP hybrid nanofluid past a permeable shrinking wedge.

1. Introduction

Non-Newtonian fluids have drawn considerable interest for their valuable industrial applications, primarily because Newtonian fluids fall short in representing the behavior of real liquids in many manufacturing processes. Various models for non-Newtonian fluids have been proposed [1].

Among them, the Reiner-Philippoff (RP) model is notable for its ability to simulate three behaviors – dilatant, shear-thinning, and shear-thickening – within a single model. Kapur and Gupta [2] applied the Karman-Pohlhausen technique to solve boundary layer (BL) equations for RP fluids in channels with varying shear stresses. Later, Cavatorta and Tonini [3] compared RP fluid behavior with other fluid types. Na [4] analyzed RP fluid behavior under Blasius boundary conditions using non-similar equations, while Yam et al. [5] studied its flow over a stretching wedge, and Ahmad et al. [6] examined flow over a stretching sheet of varying thickness. Reddy et al. [7] observed that increasing the RP fluid parameter raised temperature levels and thickened the thermal boundary layer. Further research on RP fluids across different surfaces and effects is detailed in other studies [8-12].

The study of fluid flow becomes particularly important when thermal performance is factored. Choi and Eastman [13] pioneered the use of nanosized particles to enhance fluid thermal properties. Building on this, Khanafer et al. [14] and Oztop and Abu-Nada [15] explored nanofluid flow within rectangular enclosures. To boost thermal properties even further, researchers developed hybrid nanofluids – advanced fluids created by suspending multiple types of nanoparticles uniformly within a fluid. Jana et al. [16] conducted early research on these hybrid nanocomposite particles, which exhibit superior thermal characteristics compared to standard fluids, making them highly suitable for technical and industrial applications [17, 18]. Suresh et al. [19] and Takabi and Salehi [20] highlighted how these fluids can achieve desired heat transfer rates, with additional extensive research on nanofluids detailed in references [21-25].

Recent studies document various nanomaterials, with aluminum alloy nanoparticles AA7075 and AA7072 receiving attention for their outstanding thermal, chemical, and physical properties. These characteristics make them ideal for a range of industrial applications, particularly in aerospace, where they are used in glider aircraft and rocket frames [26]. Inspired by such

studies, this research examines how hybrid nanoparticles affect RP fluid flow over a shrinking wedge. Methanol is chosen as the base fluid, with AA7075 and AA7072 as the hybrid nanoparticles. By applying a similarity transformation, the governing equations are simplified into a set of ordinary differential equations (ODEs). This study primarily identifies critical values of the physical parameters, offering insights into laminar flow separation. Stability of the solutions is analyzed, and findings for the physical parameters are presented graphically and also in tables.

2. Mathematical Formulation

The flow configuration of RP fluid over a shrinking wedge is indicated in Figure 1. The free stream and the wedge velocities are defined as $u_e(x) = ax^{1/3}$ and $u_w(x) = bx^{1/3}$, respectively, with the constants a and b. Additionally, the wedge permeability is depicted by the mass flow velocity $v_w(x)$ taken as $v_w(x) = -(2/3)\sqrt{a\nu_f}\,x^{-1/3}S$, where S is the suction parameter. Meanwhile, the magnetic field is taking transversely along the y-axis as $B(x) = B_0 x^{-1/3}$. The term B_0 is defined for constant magnetic, see reference [27]. The terms T_w and T_∞ represent constants for surface and ambient temperatures, respectively.

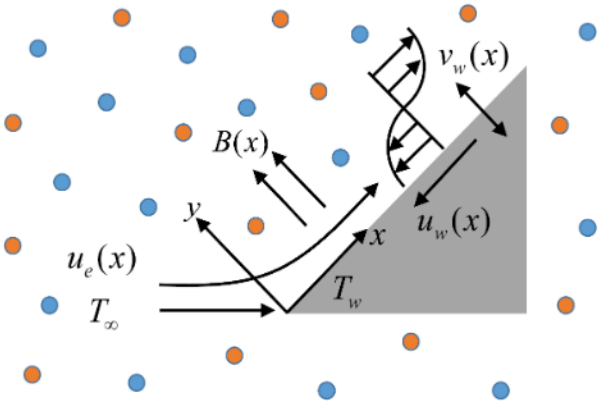

Figure 1. Physical model.

Besides, the shear stress τ associated to velocity gradient is given as:

$$\frac{\partial u}{\partial y} = \frac{\tau}{\propto_{\infty} + \dfrac{\propto_{hnf} - \propto_{\infty}}{1 + \left(\dfrac{\tau}{\tau_s}\right)^2}}, \tag{1}$$

where τ_s signifies the reference shear stress; $\propto_{\infty}$ denotes the limiting dynamic; and $\propto_0$ represents the zero-shear dynamic viscosity. Thus, the governing equations are, see references [4, 5]:

$$\frac{\partial u}{\partial x} + \frac{\partial v}{\partial y} = 0, \tag{2}$$

$$u\frac{\partial u}{\partial x} + v\frac{\partial u}{\partial y} = u_e\frac{\partial u_e}{\partial x} + \frac{1}{\rho_{hnf}}\frac{\partial \tau}{\partial y} + \frac{\sigma_{hnf}}{\rho_{hnf}}B^2(u_e - u), \tag{3}$$

$$u\frac{\partial T}{\partial x} + v\frac{\partial T}{\partial y} = \frac{k_{hnf}}{(\rho c_p)_{hnf}}\frac{\partial^2 T}{\partial y^2} \tag{4}$$

subject to

$$u = u_w(x),\ v = v_w(x),\ T = T_w \text{ at } y = 0;$$

$$u \to u_e(x),\ T \to T_{\infty} \text{ as } \eta \to \infty. \tag{5}$$

The appropriate similarity transformations (6) are adopted from references [4, 5]:

$$\psi = \sqrt{a\nu_f}\,x^{2/3} f(\eta), \quad \tau = \rho\sqrt{a^3\nu_f}\,g(\eta),$$

$$\theta(\eta) = \frac{T - T_{\infty}}{T_w - T_{\infty}}, \quad \eta = \frac{y}{x^{1/3}}\sqrt{\frac{a}{\nu_f}}. \tag{6}$$

Upon applied (6), equations (1), (3) and (4) are reduced to a set of ODEs as:

$$g = f''\left(\frac{(\alpha_{hnf}/\alpha_f)\lambda\gamma + g^2}{\gamma + g^2}\right), \tag{7}$$

$$\frac{1}{\rho_{hnf}/\rho_f} g' + \frac{2}{3} ff'' - \frac{1}{3} f'^2 + \frac{1}{3} + \frac{\sigma_{hnf}/\sigma_f}{\rho_{hnf}/\rho_f} M^2(1 - f') = 0, \tag{8}$$

$$\frac{1}{\Pr} \frac{k_{hnf}/k_f}{(\rho c_p)_{hnf}/(\rho c_p)_f} \theta'' + \frac{2}{3} f\theta' = 0 \tag{9}$$

subject to

$$f(0) = S,\ f'(0) = \varepsilon,\ \theta(0) = 1;$$

$$f'(\eta) \to 1,\ \theta(\eta) \to 0 \text{ as } \eta \to \infty \tag{10}$$

with the Prandtl number $(\Pr)$, the Reiner-Philippoff fluid number (λ), the Bingham number (γ), the magnetic parameter (M) and the stretching/shrinking parameter (ε) defined as

$$\Pr = \frac{(\alpha C_p)_f}{k_f},\ \lambda = \frac{\alpha_0}{\alpha_\infty},\ \gamma = \left(\frac{\tau_s}{\rho_f\sqrt{a^3\nu_f}}\right)^2,\ M = \sqrt{\frac{\sigma_f}{\rho_f a}}B_0,\ \varepsilon = \frac{b}{a}. \tag{11}$$

The skin friction C_f and the local Nusselt number Nu_x are given as:

$$C_f = \frac{\tau_w}{\rho_f u_e^2},\quad Nu_x = \frac{xq_w}{k_f(T_w - T_\infty)}, \tag{12}$$

where

$$\tau_w = \rho_f\sqrt{a^3\nu_f}\,(g(\eta))_{y=0},\quad q_w = -k_{hnf}\left(\frac{\partial T}{\partial y}\right)_{y=0} \tag{13}$$

at which the τ_w expresses the rate of τ at $y = 0$ and q_w as heat flux on surface. Then, the following expressions are obtained:

$$\mathrm{Re}_x^{1/2} C_f = g(0), \quad \mathrm{Re}_x^{-1/2} Nu_x = -\frac{k_{hnf}}{k_f}\theta'(0), \tag{14}$$

where $\mathrm{Re}_x = u_e(x)x/\nu_f$ is known as the local Reynolds number.

Furthermore, Table 1 provides the properties of methanol, AA7075, and AA7072. Note that, φ_1 and φ_2 denote AA7075 and AA7072 nanoparticles, respectively, where $\varphi_{hnf} = \varphi_1 + \varphi_2$. Meanwhile, the correlations of hybrid nanofluid are presented in Table 2.

Table 1. The thermophysical properties [26]

Properties	$\rho\,(\mathrm{kg/m^2})$	$C_p\,(\mathrm{J/kgK})$	$k\,(\mathrm{W/mK})$	$\sigma\,(\mathrm{S/m})$	Pr
Methanol	792	2545	0.2035	$0.5 \cdot 10^{-6}$	7.38
AA7075	2810	960	173	$26.77 \cdot 10^{6}$	
AA7072	2720	893	222	$34.83 \cdot 10^{6}$	

Table 2. Hybrid nanofluid correlations [24]

Dynamic viscosity: $\propto_{hnf} = \dfrac{\propto_f}{(1-\varphi_{hnf})^{2.5}}$
Density: $\rho_{hnf} = (1-\varphi_{hnf})\rho_f + \varphi_1\rho_{n1} + \varphi_2\rho_{n2}$
Heat viscosity: $(\rho C_p)_{hnf} = (1-\varphi_{hnf})(\rho C_p)_f + \varphi_1(\rho C_p)_{n1} + \varphi_2(\rho C_p)_{n2}$
Thermal conductivity: $\dfrac{k_{hnf}}{k_f} = \dfrac{\frac{\varphi_1 k_{n1} + \varphi_2 k_{n2}}{\varphi_{hnf}} + 2k_f + 2(\varphi_1 k_{n1} + \varphi_2 k_{n2}) - 2\varphi_{hnf} k_f}{\frac{\varphi_1 k_{n1} + \varphi_2 k_{n2}}{\varphi_{hnf}} + 2k_f - (\varphi_1 k_{n1} + \varphi_2 k_{n2}) + \varphi_{hnf} k_f}$
Electrical conductivity: $\dfrac{\sigma_{hnf}}{\sigma_f} = \dfrac{\frac{\varphi_1 \sigma_{n1} + \varphi_2 \sigma_{n2}}{\varphi_{hnf}} + 2\sigma_f + 2(\varphi_1 \sigma_{n1} + \varphi_2 \sigma_{n2}) - 2\varphi_{hnf} \sigma_f}{\frac{\varphi_1 \sigma_{n1} + \varphi_2 \sigma_{n2}}{\varphi_{hnf}} + 2\sigma_f - (\varphi_1 \sigma_{n1} + \varphi_2 \sigma_{n2}) + \varphi_{hnf} \sigma_f}$

3. Stability Analysis

As the dual solutions are obtained from computation, their stability has to be checked. The instability of results is checked by using stability analysis [28, 29].

The semi-similar variables are introduced, see Yam et al. [5]:

$$\psi = \sqrt{a\nu_f}\, x^{2/3} f(\eta, \Gamma), \quad \tau = \rho\sqrt{a^3\nu_f}\, g(\eta, \Gamma),$$

$$\theta(\eta, \Gamma) = \frac{T - T_\infty}{T_w - T_\infty}, \quad \eta = \frac{y}{x^{1/3}}\sqrt{\frac{a}{\nu_f}}, \quad \Gamma = \frac{a}{x^{2/3}}t, \tag{15}$$

where Γ is the dimensionless time variable. Then

$$u = ax^{1/3}\frac{\partial f}{\partial \eta}(\eta, \Gamma),$$

$$v = -\sqrt{a\nu_f}\, x^{-1/3}\left(\frac{2}{3}f(\eta, \Gamma) - \frac{1}{3}\eta\frac{\partial f}{\partial \eta}(\eta, \Gamma) - \frac{2}{3}\Gamma\frac{\partial f}{\partial \Gamma}(\eta, \Gamma)\right). \tag{16}$$

The unsteady forms of equations (3) and (4) can be written as:

$$\frac{\partial u}{\partial t} + u\frac{\partial u}{\partial x} + v\frac{\partial u}{\partial y} = u_e\frac{du_e}{dx} + \frac{1}{\rho_{hnf}}\frac{\partial \tau}{\partial y} + \frac{\sigma_{hnf}}{\rho_{hnf}}B^2(u_e - u), \tag{17}$$

$$\frac{\partial T}{\partial t} + u\frac{\partial T}{\partial x} + v\frac{\partial T}{\partial y} = \frac{k_{hnf}}{(\rho c_p)_{hnf}}\frac{\partial^2 T}{\partial y^2}, \tag{18}$$

while equations (1) and (2) do not change. Applying equations (15) and (16), one gets:

$$g = \frac{\partial^2 f}{\partial \eta^2}\left(\frac{(\alpha_{hnf}/\alpha_f)\lambda\gamma + g^2}{\gamma + g^2}\right), \tag{19}$$

$$\frac{1}{\rho_{hnf}/\rho_f}\frac{\partial g}{\partial \eta} + \frac{2}{3}f\frac{\partial^2 f}{\partial \eta^2} - \frac{1}{3}\left(\frac{\partial f}{\partial \eta}\right)^2 + \frac{1}{3} + \frac{\sigma_{hnf}/\sigma_f}{\rho_{hnf}/\rho_f}M^2\left(1 - \frac{\partial f}{\partial \eta}\right)$$

$$- \frac{\partial^2 f}{\partial \eta \partial \Gamma} - \frac{2}{3}\Gamma\left(\frac{\partial f}{\partial \Gamma}\frac{\partial^2 f}{\partial \eta^2} - \frac{\partial f}{\partial \eta}\frac{\partial^2 f}{\partial \eta \partial \Gamma}\right) = 0, \tag{20}$$

$$\frac{1}{\mathrm{Pr}}\frac{k_{hnf}/k_f}{(\rho c_p)_{hnf}/(\rho c_p)_f}\frac{\partial^2\theta}{\partial\eta^2}+\frac{2}{3}f\frac{\partial\theta}{\partial\eta}-\frac{\partial\theta}{\partial\Gamma}-\frac{2}{3}\Gamma\left(\frac{\partial f}{\partial\Gamma}\frac{\partial\theta}{\partial\eta}-\frac{\partial f}{\partial\eta}\frac{\partial\theta}{\partial\Gamma}\right)=0, \quad (21)$$

subject to

$$f(0,\Gamma)-\Gamma\frac{\partial f}{\partial\Gamma}(0,\Gamma)=S,\quad \frac{\partial f}{\partial\eta}(0,\Gamma)=\varepsilon,\quad \theta(0,\Gamma)=1;$$

$$\frac{\partial f}{\partial\eta}(\eta,\Gamma)\to 1,\quad \theta(\eta,\Gamma)\to 0 \text{ as } \eta\to\infty. \quad (22)$$

Next, the perturbation function is deliberated, see Weidman et al. [29]:

$$f(\eta,\Gamma)=f_0(\eta)+e^{-\alpha\Gamma}F(\eta,\Gamma),$$

$$g(\eta,\Gamma)=g_0(\eta)+e^{-\alpha\Gamma}G(\eta,\Gamma),$$

$$\theta(\eta,\Gamma)=\theta_0(\eta)+e^{-\alpha\Gamma}H(\eta,\Gamma), \quad (23)$$

where $F(\eta,\Gamma)$, $G(\eta,\Gamma)$ and $H(\eta,\Gamma)$ are arbitrary functions and smaller than $f_0(\eta)$, $g_0(\eta)$ and $\theta_0(\eta)$, and α indicates the eigenvalue. Let $\Gamma=0$. Then $F(\eta,\Gamma)=F_0(\eta)$, $G(\eta,\Gamma)=G_0(\eta)$ and $H(\eta,\Gamma)=H_0(\eta)$. The linearization of the eigenvalue problems is as follows:

$$G_0=F_0''\left(\frac{(\propto_{hnf}/\propto_f)\lambda\gamma+g_0^2}{\gamma-2f_0''g_0+3g_0^2}\right), \quad (24)$$

$$\frac{1}{\rho_{hnf}/\rho_f}G_0'+\frac{2}{3}(f_0F_0''+f_0''F_0)-\frac{2}{3}f_0'F_0'-\frac{\sigma_{hnf}/\sigma_f}{\rho_{hnf}/\rho_f}M^2F_0'+\alpha F_0'=0, \quad (25)$$

$$\frac{1}{\mathrm{Pr}}\frac{k_{hnf}/k_f}{(\rho c_p)_{hnf}/(\rho c_p)_f}H_0''+\frac{2}{3}(f_0H_0'+\theta_0'F_0)+\alpha H_0=0, \quad (26)$$

subject to

$$F_0(0)=0,\ F_0'(0)=0,\ H_0(0)=0;$$

$$F_0'(\eta)\to 0,\ H_0(\eta)\to 0 \text{ as } \eta\to\infty. \quad (27)$$

In order to acquire α from equations (24)-(26), $F_0'(\eta) \to 0$ as $\eta \to \infty$ in equation (27) is replaced with $F''(0) = 1$, see Harris et al. [30].

4. Results and Discussion

The results of the numerical computation are discussed in this segment. The bvp4c solver embedded in Matlab software is used in computing equations (8)-(10), see reference [31].

Table 3. Values of $\mathrm{Re}_x^{1/2} C_f$ for regular fluid case $(\varphi_1 = \varphi_2 = 0)$ when $S = M = 0$ and $\gamma = 1$

λ	$\varepsilon = -0.95$		$\varepsilon = -0.995$	
	Present result	Yam et al. [5]	Present result	Yam et al. [5]
0.1	0.174047	0.1740	0.113773	0.1138
0.6	0.426436	0.4264	0.282519	0.2825
1	0.546695	0.5470	0.367218	0.3672
1.8	0.717538	0.7175	0.495286	0.4953
2.6	0.841255	0.8412	0.594055	0.5940

The output of $\mathrm{Re}_x^{1/2} C_f$ for regular fluid case $(\varphi_1 = \varphi_2 = 0)$ without the effect of S and M at $\gamma = 1$ is presented in Table 3. The quantity of $\mathrm{Re}_x^{1/2} C_f$ is amplified in aggregate of λ and ε, respectively. Additionally, the output established by Yam et al. [5] is being compared, and excellent agreement is attained. This evident supports the soundness, accuracy, and precision of the current model and its numerical outcomes.

Tables 4 and 5 provide the values of $\mathrm{Re}_x^{1/2} C_f$ and $\mathrm{Re}_x^{-1/2} Nu_x$ for various types of fluids with distinct values of M when $\lambda = S = 0.5$, $\gamma = 1$, $\mathrm{Pr} = 7.38$ and $\varepsilon = -1.25$ (shrinking wedge), respectively. From these

tables, the values of $\mathrm{Re}_x^{1/2} C_f$ and $\mathrm{Re}_x^{-1/2} Nu_x$ are increased in growing values of M. Comparable behavior is detected for the effect of added nanoparticle on these physical quantities. For fixed value of $M = 0$, there are 2.97% and 3.13% increments in $\mathrm{Re}_x^{1/2} C_f$ for AA7072/methanol $(\varphi_1 = 0, \varphi_2 = 0.01)$ and AA7075/methanol $(\varphi_1 = 0.01, \varphi_2 = 0)$, respectively, if compared to methanol $(\varphi_1 = \varphi_2 = 0)$. These increments are more pronounced for AA7075-AA7072/methanol $(\varphi_1 = \varphi_2 = 0.01)$ with 6.16%. Besides, the heat transfer of the base fluid is improved by considering the nanoparticle with 11.25% and 12.06% increments for AA7072/methanol and AA7075/methanol, respectively. Meanwhile, 24% increment of $\mathrm{Re}_x^{-1/2} Nu_x$ is observed for AA7075-AA7072/methanol.

Figures 2 and 3 demonstrate how the parameter M affects the quantity of $\mathrm{Re}_x^{1/2} C_f$ and $\mathrm{Re}_x^{-1/2} Nu_x$. Both of physical quantities are heightened in growing of magnetic rate. As demonstrated in Figure 2, the intensifying of Lorentz force induced from magnetic field retarded the flow field whilst delaying the BL separation. It can be seen that the critical values are expanded, which are given by $\varepsilon_{c1} = -1.2716 (M = 0)$, $\varepsilon_{c2} = -1.2896 (M = 0.1)$ and $\varepsilon_{c3} = -1.3441 (M = 0.2)$. In addition, Figure 3 reveals the enlargement in the value of magnetic parameter which advanced heat transfer in the fluid.

According to the first solution in Figure 4, the free stream flow helps to stabilise the free vorticity within the opposing flow induced by shrinking which led to increase the fluid velocity. In particular, the availability of magnetic strength progresses the fluid movement which then pushes the hot particles in the direction of the plate. As seen in Figure 5, this activity increases heat transport while lowering the temperature distribution.

The deviations on the smallest eigenvalues are shown in Figure 6, where the positive eigenvalue provided the first solution and the negative eigenvalue provided the second. The first solution is therefore stable and significantly realisable, whereas the second solution behaves in the opposite way.

Table 4. Values of $\mathrm{Re}_x^{1/2} C_f$ for various types of fluids with distinct values of M when $\lambda = S = 0.5$, $\gamma = 1$, $\mathrm{Pr} = 7.38$ and $\varepsilon = -1.25$ (shrinking wedge)

M	Methanol	AA7072/methanol	AA7075/methanol	AA7075-AA7072/methanol
0	0.620163	0.638563	0.639572	0.658338
0.05	0.636388	0.655216	0.656176	0.675386
0.1	0.678986	0.698970	0.699840	0.720242
0.2	0.808132	0.831666	0.832405	0.856410

Table 5. Values of $\mathrm{Re}_x^{-1/2} Nu_x$ for various types of fluids with distinct values of M when $\lambda = S = 0.5$, $\gamma = 1$, $\mathrm{Pr} = 7.38$ and $\varepsilon = -1.25$ (shrinking wedge)

M	Methanol	AA7072/methanol	AA7075/methanol	AA7075-AA7072/ methanol
0	0.101182	0.112561	0.113387	0.125467
0.05	0.115357	0.127673	0.128503	0.141534
0.1	0.155643	0.170318	0.171166	0.186574
0.2	0.293529	0.313953	0.314885	0.335998

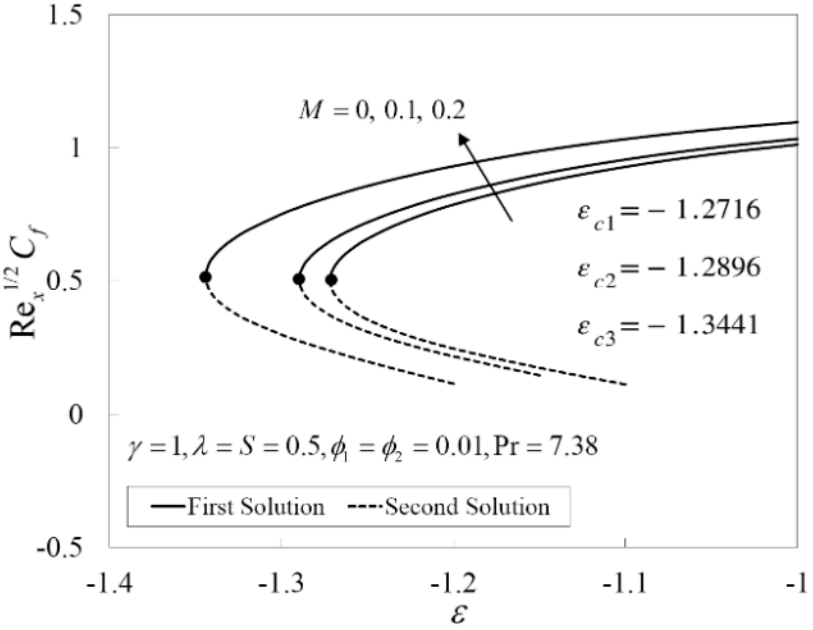

Figure 2. $\mathrm{Re}_x^{1/2} C_f$ vs ε and M.

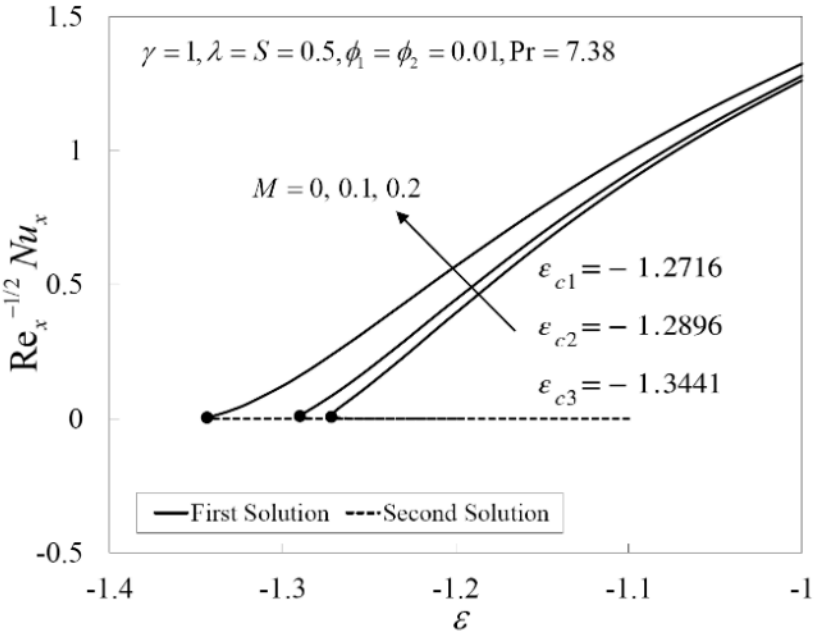

Figure 3. $\mathrm{Re}_x^{-1/2} Nu_x$ vs ε and M.

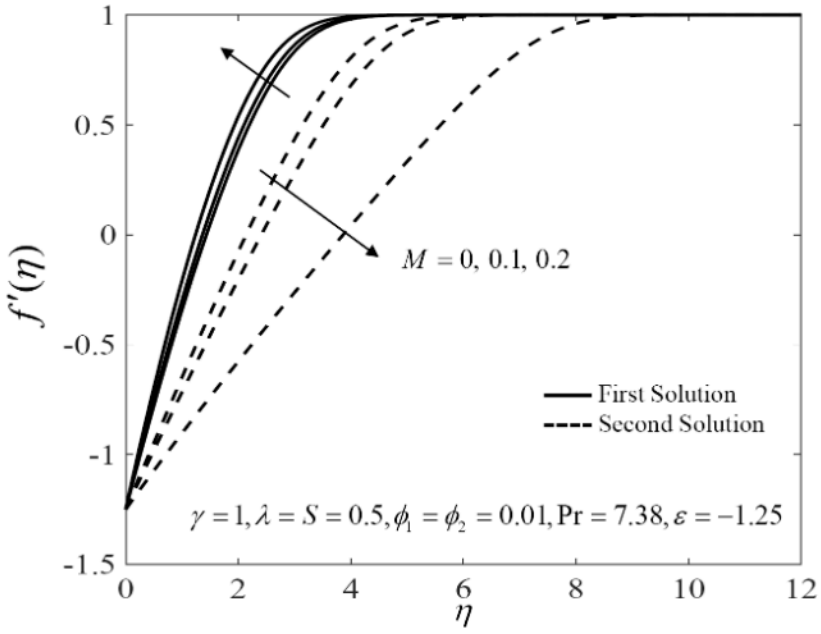

Figure 4. $f'(\eta)$ vs M.

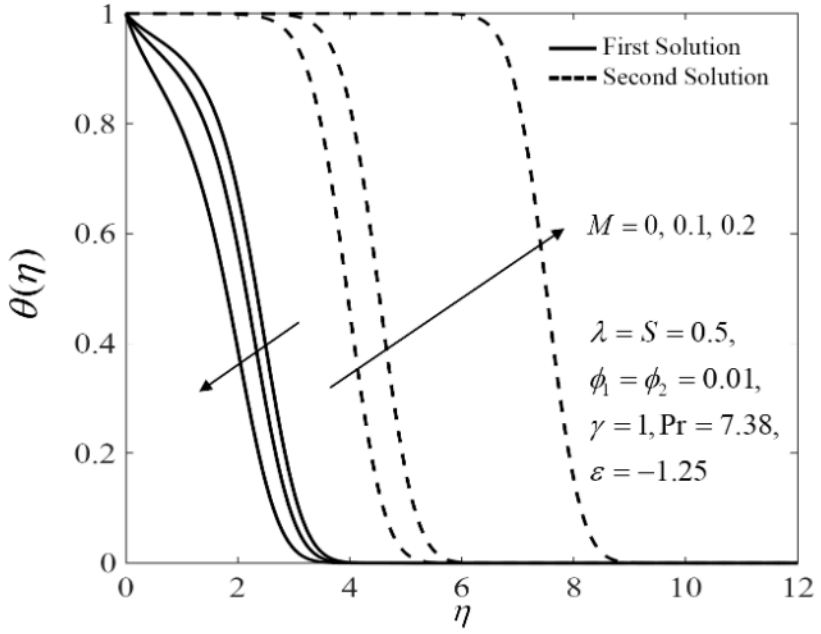

Figure 5. $\theta(\eta)$ vs M.

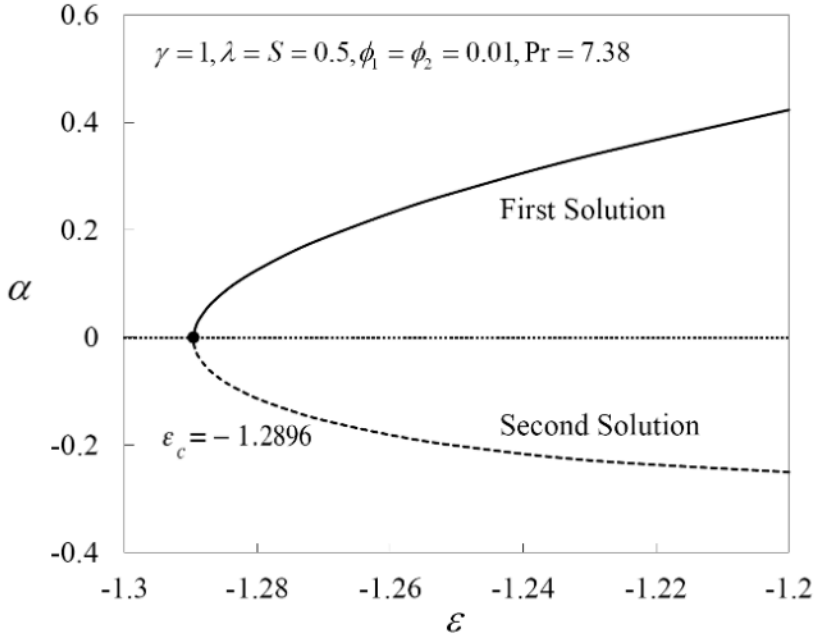

Figure 6. α vs ε.

5. Conclusions

This research is centered on examining the steady flow of RP fluid on shrinking wedge contained hybrid nanoparticles. To solve the proposed model, a similarity transformation is employed to change the governing equations, and subsequently, the numerical solution is obtained using the bvp4c solver. According to the findings, hybrid nanofluids demonstrate remarkable thermal conductivity and significantly enhance the heat transport. Specifically, the heat transfer rate is increased by 11.25% and 12.06% for AA7072/methanol and AA7075/methanol, respectively. Meanwhile, 24% increment is for AA7075-AA7072/methanol if compared to the base fluid (methanol). These findings show how hybrid nanofluids aid in effective heat transport. Larger magnetic parameters are also seen to increase skin friction and heat transfer rate. The first solution is verified stable and practical, while the second solution displays the opposite decision.

Acknowledgement

We appreciate the financial supports from Universiti Teknikal Malaysia Melaka (JURNAL/2022/FTKIP/Q00088).

References

[1] A. P. Deshpande, J. M. Krishnan and P. B. S. Kumar, Rheology of Complex Fluids, Springer, New York, 2010.

[2] J. N. Kapur and R. C. Gupta, Two dimensional flow of Reiner-Philippoff fluids in the inlet length of a straight channel, Applied Scientific Research 14 (1964), 13-24.

[3] O. N. Cavatorta and R. D. Tonini, Dimensionless velocity profiles and parameter maps for non-Newtonian fluids, International Communications in Heat and Mass Transfer 14 (1987), 359-369.

[4] T. Y. Na, Boundary layer flow of Reiner-Philippoff fluids, Internat. J. Non-Linear Mech. 29 (1994), 871-877.

[5] K. S. Yam, S. D. Harris, D. B. Ingham and I. Pop, Boundary-layer flow of Reiner-Philippoff fluids past a stretching wedge, Internat. J. Non-Linear Mech. 44 (2009), 1056-1062.

[6] A. Ahmad, M. Qasim and S. Ahmed, Flow of Reiner-Philippoff fluid over a stretching sheet with variable thickness, Journal of the Brazilian Society of Mechanical Sciences and Engineering 39 (2017), 4469-4473.

[7] M. G. Reddy, M. V. V. N. L. Sudharani, K. Ganesh Kumar, A. J. Chamkha and G. Lorenzini, Physical aspects of Darcy-Forchheimer flow and dissipative heat transfer of Reiner-Philippoff fluid, J. Therm. Anal. Calorim. 141 (2020), 829-838.

[8] T. Sajid, S. Tanveer, M. Munsab and Z. Sabir, Impact of oxytactic microorganisms and variable species diffusivity on blood-gold Reiner-Philippoff nanofluid, Appl. Nanosci. 11 (2021), 321-333.

[9] A. Ullah, E. O. Alzahrani, Z. Shah, M. Ayaz and S. Islam, Nanofluids thin film flow of Reiner-Philippoff fluid over an unstable stretching surface with Brownian motion and thermophoresis effects, Coatings 9 (2019), 21.

[10] M. Tahir and A. Ahmad, Impact of pseudoplaticity and dilatancy of fluid on peristaltic flow and heat transfer: Reiner-Philippoff fluid model, Advances in Mechanical Engineering 12 (2020), 1-10.

[11] I. Waini, K. Bin Hamzah, S. Khashi'ie, A. Zainal, A. Rahman, M. Kasim, A. Ishak and I. Pop, Brownian and thermophoresis diffusion effects on magnetohydrodynamic Reiner-Philippoff nanofluid flow past a shrinking sheet, Alexandria Engineering Journal 67 (2023), 183-192.

[12] I. Waini, N. A. Zainal, N. S. Khashi'ie, K. Bin Hamzah, A. R. M. Kasim, A. Ishak and I. Pop, Mixed convection of MHD Reiner-Philippoff fluid flow past a vertical shrinking plate with radiative heat transfer, Chinese J. Phys. 83 (2023), 325-336.

[13] S. U. S. Choi and J. A. Eastman, Enhancing thermal conductivity of fluids with nanoparticles, Proceedings of the 1995 ASME International Mechanical Engineering Congress and Exposition, FED 231/MD. 66 (1995), 99-105.

[14] K. Khanafer, K. Vafai and M. Lightstone, Buoyancy-driven heat transfer enhancement in a two-dimensional enclosure utilizing nanofluids, Int. J. Heat Mass Transf. 46 (2003), 3639-3653.

[15] H. F. Oztop and E. Abu-Nada, Numerical study of natural convection in partially heated rectangular enclosures filled with nanofluids, Int. J. Heat Fluid Flow. 29 (2008), 1326-1336.

[16] S. Jana, A. Salehi-Khojin and W. H. Zhong, Enhancement of fluid thermal conductivity by the addition of single and hybrid nano-additives, Thermochim. Acta 462 (2007), 45-55.

[17] J. A. R. Babu, K. K. Kumar and S. S. Rao, State-of-art review on hybrid nanofluids, Renewable and Sustainable Energy Reviews 77 (2017), 551-565.

[18] N. A. C. Sidik, I. M. Adamu, M. M. Jamil, G. H. R. Kefayati, R. Mamat and G. Najafi, Recent progress on hybrid nanofluids in heat transfer applications: a comprehensive review, International Communications in Heat and Mass Transfer 78 (2016), 68-79.

[19] S. Suresh, K. P. Venkitaraj, P. Selvakumar and M. Chandrasekar, Synthesis of Al_2O_3-Cu/water hybrid nanofluids using two step method and its thermo physical properties, Colloids Surf A Physicochem. Eng. Asp. 388 (2011), 41-48.

[20] B. Takabi and S. Salehi, Augmentation of the heat transfer performance of a sinusoidal corrugated enclosure by employing hybrid nanofluid, Advances in Mechanical Engineering 6 (2014), 147059.

[21] I. Waini, A. Ishak and I. Pop, Hybrid nanofluid flow on a shrinking cylinder with prescribed surface heat flux, Int. J. Numer. Methods Heat Fluid Flow 31 (2021), 1987-2004.

[22] I. Waini, A. Ishak and I. Pop, Hybrid nanofluid flow over a permeable non-isothermal shrinking surface, Mathematics 9 (2021), 538.

[23] I. Waini, A. Ishak and I. Pop, Symmetrical solutions of hybrid nanofluid stagnation-point flow in a porous medium, International Communications in Heat and Mass Transfer 130 (2022), 105804.

[24] A. K. Pati, A. Misra, S. K. Mishra, S. Mishra, R. Sahu and S. Panda, Computational modelling of heat and mass transfer optimization in copper water nanofluid flow with nanoparticle ionization, JP Journal of Heat and Mass Transfer 31 (2023), 1-18.

[25] N. A. Rahman, N. S. Khashi'ie, K. B. Hamzah, N. A. Zainal, I. Waini and I. Pop, Axisymmetric hybrid nanofluid flow over a radially shrinking disk with heat generation and magnetic field effects, JP Journal of Heat and Mass Transfer 37(3) (2024), 365-375.

[26] I. Tlili, H. A. Nabwey, G. P. Ashwinkumar and N. Sandeep, 3-D magnetohydrodynamic AA7072-AA7075/methanol hybrid nanofluid flow above an uneven thickness surface with slip effect, Sci. Rep. 10 (2020), 1-13.

[27] K. G. Kumar, M. G. Reddy, M. V. V. N. L. Sudharani, S. A. Shehzad and A. J. Chamkha, Cattaneo-Christov heat diffusion phenomenon in Reiner-Philippoff fluid through a transverse magnetic field, Phys. A 541 (2020), 123330.

[28] J. H. Merkin, On dual solutions occurring in mixed convection in a porous medium, J. Eng. Math. 20 (1986), 171-179.

[29] P. D. Weidman, D. G. Kubitschek and A. M. J. Davis, The effect of transpiration on self-similar boundary layer flow over moving surfaces, Internat. J. Engrg. Sci. 44 (2006), 730-737.

[30] S. D. Harris, D. B. Ingham and I. Pop, Mixed convection boundary-layer flow near the stagnation point on a vertical surface in a porous medium: Brinkman model with slip, Transp. Porous Media 77 (2009), 267-285.

[31] L. F. Shampine, I. Gladwell and S. Thompson, Solving ODEs with MATLAB, Cambridge University Press, Cambridge, 2003.